A Novel Implementation of Berenger's PML for FDTD Applications

Funda Akleman, *Student Member, IEEE,* and Levent Sevgi

***Abstract*— In this letter, a new implementation of the three-dimensional (3-D) perfectly matched layer (PML) in finite-difference time-domain (FDTD) applications is introduced. This technique is based on doubling the cell dimensions in PML region where extra averaging of electrical field components are necessary at the edges and faces along the PML–FDTD interfaces. The presented numerical examples are for 3-D structures which exhibit complex wave phenomena. Significant improvement obtained after this implementation, especially at lower frequencies, is demonstrated.**

***Index Terms*—Absorbing boundary condition, finite-difference time-domain method, perfectly matched layer.**

I. Introduction

APPLICATION of absorbing boundary conditions (ABC'S) to simulate open regions has been one of the key issues in finite-difference time-domain (FDTD) calculations. Recently, Berenger [1] introduced a novel technique called perfectly matched layer (PML) which offers excellent absorbing performance in FDTD applications. It is based on covering the FDTD volume with a fictitious region where directionally dependent pair of electric and magnetic conductivities are introduced to absorb outgoing waves. Since then, various modifications have appeared in numerical applications. Among these are using unsplit PML [2] or electric displacement instead of electric field [3], making improvements to absorb evanescent waves [4], [5], and extending the technique to match dielectric on isotropic media [6] and dispersive media [7]. Also, noncubic cell [8], modal [9], and modified [10] type PML techniques have appeared in the literature.

In this letter, the Berenger's PML is implemented to minimize the memory and computational requirements as well as to obtain better absorbing performance, especially at lower frequencies. Both Berenger's PML and its new implementation presented here display the same robust characteristics. Therefore, detailed parameter tests and optimization are not included. Instead, numerical examples are chosen for three-dimensional (3-D) complex structures and the results are compared for broad range of frequencies.

Manuscript received May 6, 1998.

F. Akleman is with the Electronics and Communication Engineering Department, İTÜ, 80626 Maslak/Istanbul, Turkey.

L. Sevgi is with Raytheon Canada Limited, Waterloo, Ont. N2J 4K6 Canada, on leave from the Electronics and Communication Engineering Department, İTÜ, 80626 Maslak/Istanbul, Turkey.

Publisher Item Identifier S 1051-8207(98)08661-9.

II. Berenger's PML and Its Novel Implementation

The original Berenger's PML results in 12 split field equations in 3-D, two of which are given below

$$\mu_0\frac{\partial H_{zx}}{\partial t}+\sigma_x^* H_{zx}=-\frac{\partial(E_{yx}+E_{yz})}{\partial x} \tag{1}$$

$$\mu_0\frac{\partial H_{zy}}{\partial t}+\sigma_y^* H_{zy}=\frac{\partial(E_{xy}+E_{xz})}{\partial y}. \tag{2}$$

The condition for the reflectionless absorption is

$$\frac{\sigma_i}{\varepsilon}=\frac{\sigma_i^*}{\mu}\quad i=x,y,z \tag{3}$$

which is independent of angle of incidence or frequency. The reflection is a function of $\sigma\times d$ (i.e., conductivity multiplied by PML depth). The depth of the PML region (i.e., number of PML layers) may arbitrarily be chosen but not the conductivity. Assigning a constant value to σ may cause strong reflections because of a sharp conductivity transition at FDTD–PML interface. A well-accepted choice for conductivity profile in PML region is [1]

$$\sigma(\rho)=\sigma_{\max}\left(\frac{\rho}{d}\right)^n \tag{4}$$

where

- $\sigma_{\max}$ maximum conductivity value;
- d entire PML depth;
- n order of spatial polynomial;
- ρ distance in PML region from FDTD–PML interface.

The spatial decay of the field inside PML region is mainly controlled by $\sigma_{\max}$ which may be chosen as

$$\sigma_{\max}=\frac{(n+1)\varepsilon_o c}{2d}\ln\left(\frac{1}{R}\right) \tag{5}$$

for a given theoretical value of reflection coefficient (R) at normal incidence. For this exponential conductivity profile, first, the number (m) of PML layers (i.e., the PML cell size, Δ_{PML}) and the reflection coefficient are chosen. Then, $\sigma_{\max}$ from (5) and $\sigma_i(i=1,2,\cdots,m)$ from (4) are determined where continuous distribution of $\sigma(\rho)$ is staircased based on m. Whatever the conductivity profile in PML region, the sizes of PML and FDTD cells are same in all applications.

The performance of PML with exponential conductivity profile may be improved by using larger cell size in the PML region. The larger the PML layer depth the higher the decay of fields in a PML layer. One should be very careful while applying central-differencing at FDTD–PML interfaces if different cell sizes are chosen in FDTD and PML regions.

1051–8207/98$10.00 © 1998 IEEE

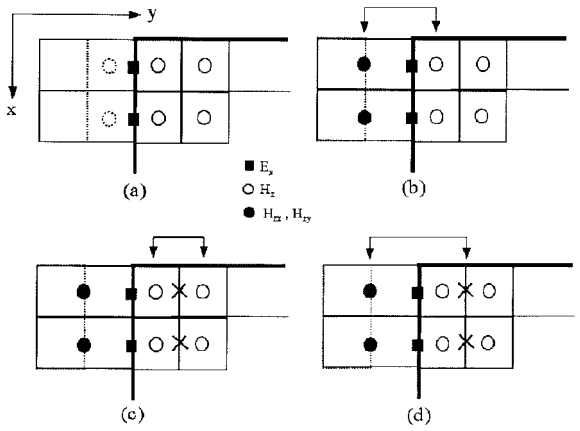

Fig. 1. FDTD–PML interface and field locations (right: FDTD; left: PML). (a) Equally separated magnetic fields (circles) which are used to calculate the electric fields (squares) at the interface. (b) Two magnetic fields are no longer equidistant when the PML layer size is doubled in the y direction. (c) Two inner magnetic fields are averaged to make an equidistant pair to the magnetic field in the PML region. (d) The pair of magnetic fields which are used to calculate the electric field at the interface.

In Fig. 1, the FDTD–PML interface is shown in an xy plane for any $z = \text{constant}$, together with the locations of field components. The thick line is the interface which separates the FDTD region from the PML. As shown in Fig. 1(a), the two equidistant magnetic fields are used to calculate the electric field at the interface. Since the PML cell size in y direction is doubled, the two magnetic fields on both sides of the interface are no longer equally separated [see Fig. 1(b)]. To overcome this, the two magnetic fields nearest the interface in the FDTD region are first averaged [see Fig. 1(c)] and then the electric fields at the interface is calculated from the magnetic fields, as shown in Fig. 1(d). Since almost no propagation occurs toward the PML–PML interfaces, the same procedure at these interfaces are not taken into account.

As indicated in the literature, the performance strongly depends on the parameters $\sigma_{\max}$, n, Δ_{PML}, and m. In the following examples, numerical tests are carried out for various set of Δ_{PML} and m values. It should be mentioned that extra performance improvements in both our and Berenger's PML implementations shall be obtained if the parameters (such as $\sigma_{\max}$ and n) are optimized.

III. Numerical Examples

Three different structures are simulated within FDTD volume [11] to show the effectiveness of novel PML technique. For all these examples maximum conductivity and order of spatial polynomial are taken as $\sigma_{\max} = 10$ [S/m] (i.e., $R = 5.0e-3$) and $n = 2$, respectively. First, a thin wire antenna, fed by a (first derivative of a Gaussian) pulse, is located within FDTD volume of $50 \times 50 \times 50$ cells with $\Delta x = \Delta y = \Delta z = 0.125$ mm. The length of the antenna is $l = 20\Delta z$ ($l = \lambda/2$ at 60 GHz) and is located along z axis. The FDTD volume is enclosed by an eight-cell PML region, and frequency variation of unwanted reflections for both implementations are plotted in Fig. 2. The legends *Fun-n* and *Ber-n* (n is an integer) in this and the rest of the figures stand for our and Berenger's n-cell PML results, respectively.

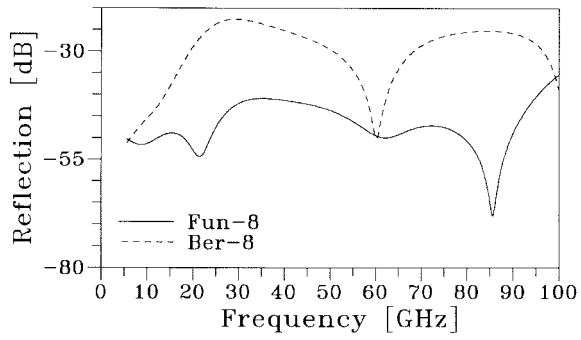

Fig. 2. Unwanted reflections in the simulation of a thin-wire dipole ($\lambda/2$ at 60 GHz) in free space.

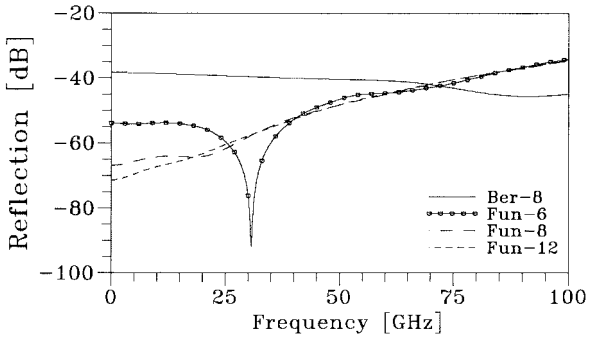

Fig. 3. Unwanted reflections near $z = Z_{\max}$ under the strip where dominant energy propagation occurs (near the longitudinal PML region).

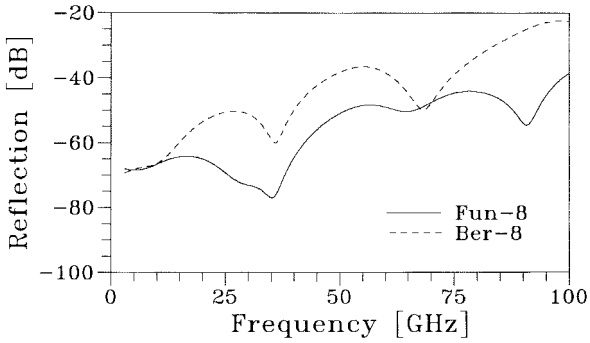

Fig. 4. Unwanted reflections near $y = Y_{\max}$ at the side PML walls of the microstrip where weak energy leakage occurs.

As clearly seen in this figure, doubling the PML cell size results in an average of 15–20-dB increase in performances in this electromagnetic radiation problem. The same calculation is repeated for multiwire antenna systems, and the effects of directivity onto PML absorbtion are tested. It is observed that the PML performances for both implementations increase since most of the energy propagate toward the PML walls.

Second, a simple microstrip line is taken into account which needs special care [12] and exhibits complex wave phenomenna. The microstrip line is located along the z axis (x is the transverse distance and y is the height) and is excited with a Gaussian pulse. A $44 \times 20 \times 60$ FDTD space is chosen with $\Delta x = \Delta y = \Delta z = 0.125$ mm cubic cell sizes. The width and height of the strip are 1 and 0.5 mm, respectively, and $\varepsilon_r = 4$ for the dielectric substrate. The frequency variation of the unwanted reflections during the

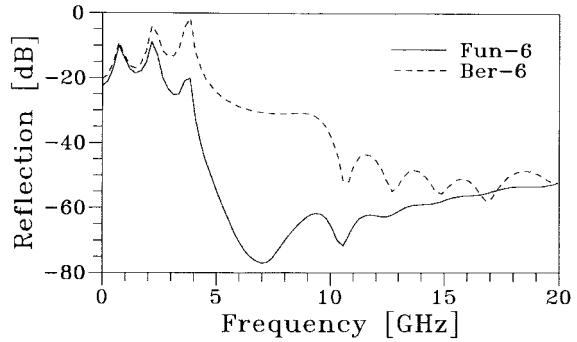

Fig. 5. Unwanted reflections near the FDTD–PML interface along the rectangular X-band waveguide.

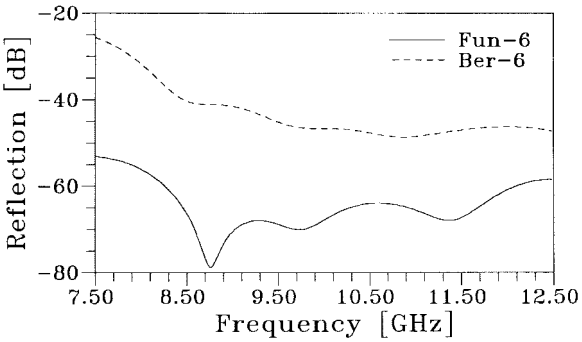

Fig. 6. Unwanted reflections near the FDTD–PML interface along the rectangular X-band waveguide for a band-limited propagation.

pulse propagation is given in Figs. 3 and 4, for transverse and longitudinal-to-strip FDTD–PML interfaces, respectively. In Fig. 3, an average of -40-dB reflections occur for Berenger's PML, but up to 30-dB improvements are obtained with the new implementation for longitudinal propagation. Similarly, better performance is obtained at the FDTD–PML interface for the transverse energy leakage as shown in Fig. 4.

Finally, unwanted reflections are analyzed inside a rectangular waveguide [9]. An X-band waveguide is terminated with six-cell PML layers on both sides and the propagation of the dominant mode is simulated which has a Gaussian pulse time behavior (with 40-GHz bandwidth). The cross section of the waveguide is chosen as 46×20. The length of the waveguide is chosen as 210 and 650 for total and incident wave observations, respectively. FDTD space is chosen with $\Delta x = \Delta y = \Delta z = 0.5$ mm cubic cell sizes [9]. The frequency variation of unwanted reflections near FDTD–PML interface is given in Fig. 5. Again, better performance obtained in this case is clearly seen in the figure. As mentioned in [9], inefficiency of PML layers to absorb evanescent waves cause oscillatory behavior in time domain, which means one should be carefull when applying Fourier transforms. Here, windowing followed by zero-padding is applied to the time variations in order to obtain the necessary frequency resolution as well as to get rid of the aliasing effects. The better performance obtained with the new implementation, especially at the low-frequency region, is shown in this figure. The last example shown in Fig. 6 belongs to the same waveguide test but for a different excitation. A Gaussian pulse (with 5-GHz bandwidth) is modulated by a $f_o = 10$ GHz carrier (i.e., a sine wave), and the reflection coefficient is calculated for the dominant mode propagation case. More stable frequency variation of unwanted reflections for both cases is obtained for this band-limited excitation in propagation region. Again, better performance is obtained with the new implementation presented here.

IV. Conclusion

In this letter, a novel implementation of Berenger's PML has been presented. The Berenger's PML performance may be obtained with a fewer number of PML layers, which means a substantial decrease in both memory and computation time requirements. A serious disadvantage of this implementation is the numerical dispersion effects. Since the cell size of PML is larger than FDTD, one should take the PML cell sizes into account for numerical dispersion. Further improvements may be obtained if the depth of each PML layer is optimized to cause maximum absorbtion [13], [14].

References

[1] J. P. Berenger, "A perfectly matched layer for the absorption of electromagnetic waves," *J. Comput. Phys.*, vol. 114, pp. 185–200, 1994.
[2] D. M. Sullivan, "An unsplit step 3-D PML for use with the FDTD method," *IEEE Microwave Guided Wave Lett.*, vol. 7, pp. 184–186, July 1997.
[3] ——, "A simplified PML for use with the FDTD method," *IEEE Microwave Guided Wave Lett.*, vol. 6, pp. 97–99, Feb. 1996.
[4] J. D. Moerloose and M. A. Stuchly, "Behavior of Berenger's ABC for evanescent waves," *IEEE Microwave Guided Wave Lett.*, vol. 5, pp. 344–346, Oct. 1995.
[5] Z. Wu and J. Fang, "Numerical implementation and performance of perfectly matched layer boundary condition for waveguide structures," *IEEE Trans. Microwave Theory Tech.*, vol. 43, pp. 2676–2683, Dec. 1995.
[6] I. V. Perez, S. G. Garcia, R. G. Martin, and B. G. Olmeda, "Extension of Berenger's absorbing boundary conditions to match dielectric anisotropic media," *IEEE Microwave Guided Wave Lett.*, vol. 7, pp. 302–304, Sept. 1997.
[7] T. Uno, Y. He, and S. Adachi, "Perfectly matched layer absorbing boundary condition for dispersive medium," *IEEE Microwave Guided Wave Lett.*, vol. 7, pp. 264–266, Sept. 1997.
[8] N. Harada and M. Hano, "PML absorbing boundary condition for noncubic cell time-domain method," *IEEE Microwave Guided Wave Lett.*, vol. 7, pp. 335–337, Oct. 1997.
[9] M. Okoniewski, M. A. Stuchly, M. Mrozowski, and J. DeMoerloose, "Modal PML," *IEEE Microwave Guided Wave Lett.*, vol. 7, pp. 33–35, Feb. 1997.
[10] B. Chen, D. G. Fang, and B. H. Zhou, "Modified Berenger PML absorbing boundary condition for FD-TD meshes," *IEEE Microwave Guided Wave Lett.*, vol. 5, pp. 399–401, Nov. 1995.
[11] L. Sevgi and S. Paker, "FDTD based RCS calculations and antenna simulations," *AEU Int. J. Electron. Commun.*, pp. 65–75, Mar. 1998.
[12] M. Chen, B. Houshmand, and T. Itoh, "FDTD analysis of a metal-strip-loaded dielectric leaky-wave antenna," *IEEE Trans. Antennas Propagat.*, vol. 45, pp. 1294–1301, Aug. 1997.
[13] F. Akleman and L. Sevgi, "FDTD analysis of human head—Mobile phone interaction in terms of specific absorbtion rate calculations and antenna simulations," to be presented at the IEEE-APS Conference on Antennas and Propagation for Wireless Communications, Waltham, MA, Nov. 2–4, 1998.
[14] F. Akleman and L. Sevgi, "Radar cross section and antenna modeling with FDTD method," to be presented at JINA'98, 10th International Symposium on Antennas, Nice, France, Nov. 14–16, 1998.